LBL-16298

# Lawrence Berkeley Laboratory
UNIVERSITY OF CALIFORNIA

## Materials & Molecular Research Division

LBL--16298

DE84 002899

To be presented at the Brookhaven Conference, Advances in Soft X-Ray Science and Technology, Brookhaven National Laboratory, Upton, NY, October 17-20, 1983

*ANGLE-RESOLVED PHOTOEMISSION EXTENDED FINE STRUCTURE*

J.J. Barton, C.C. Bahr, Z. Hussain, S.W. Robey, L.E. Klebanoff, and D.A. Shirley

September 1983

**DISCLAIMER**

This report was prepared as an account of work sponsored by an agency of the United States Government. Neither the United States Government nor any agency thereof, nor any of their employees, makes any warranty, express or implied, or assumes any legal liability or responsibility for the accuracy, completeness, or usefulness of any information, apparatus, product, or process disclosed, or represents that its use would not infringe privately owned rights. Reference herein to any specific commercial product, process, or service by trade name, trademark, manufacturer, or otherwise does not necessarily constitute or imply its endorsement, recommendation, or favoring by the United States Government or any agency thereof. The views and opinions of authors expressed herein do not necessarily state or reflect those of the United States Government or any agency thereof.

Prepared for the U.S. Department of Energy under Contract DE-AC03-76SF00098

LBL-16298

# Angle-Resolved Photoemission Extended Fine Structure

J.J. Barton, C.C. Bahr, Z. Hussain,* S.W. Robey, L.E. Klebanoff, and D.A. Shirley

Materials and Molecular Research Division, Lawrence Berkeley Laboratory,
and Departments of Chemistry and Physics, University of California
Berkeley, California 94720

## Abstract

Core level angle-resolved photoemission intensity oscillates sinusoidally with increasing photoelectron momentum. Interference between direct and scattered photoemission causes this angle-resolved photoemission extended fine structure (ARPEFS). We will discuss an analytic single-scattering theory which quantitatively describes the oscillations. The procedures for extracting surface geometry information from photoemission measurements will be illustrated with S(1s) ARPEFS from S on Ni(100) and Cu(100) obtained with the soft X-ray double crystal monochromator at the Stanford Synchrotron Radiation Laboratory. Building on the surface sensitivity and chemical selectivity of photoemission, ARPEFS analysis provides direct geometrical information from the oscillation frequencies (derived with auto-regressive Fourier analysis), from intensity changes with polarization and analyzer position, and from analysis of scattering phase-shift zero-crossings.

## Introduction

Developing practical methods for surface structure determination has been an important goal of synchrotron radiation research, particularly in the UV and soft X-ray energy range. One of the first avenues explored for structural methods was the interesting photoelectron diffraction effect[1-3]. These large modulations in the differential partial cross-section from adsorbate core levels are caused[4-6] by interference between direct and ion-core scattered photoelectron waves. While a number of surface structures have been studied with photoelectron diffraction[7], progress has been slow both because synchrotron radiation is necessary for the measurements and because indirect comparison to theory[6] has been required to determine structures.

Now a new direct-analysis approach to surface structure determination with photoelectron diffraction has been developed. We have demonstrated[8] that photoemission measurements can be analyzed to give a Fourier spectrum with peaks for individual scattering atoms. The peak positions give a scattering path length and the peak area gives a scattering power- both the position and intensity give clues to structure.

We distinguish this new approach by calling it angle-resolved photoemission extended fine structure (ARPEFS). Key ingredients include wide (500 eV) kinetic energy range measurements, facilitated by the SSRL Jumbo monochromator[9], auto-regressive (maximum entropy) Fourier transformation methods[10], and analytic single scattering theory for interpretation[11,12]. Recently, we summarized[13] our first examples of ARPEFS measurements and analysis on the surface systems c(2x2)S/Ni(100) and p(2x2)S/Cu(100), highlighting the variety of structural information available from this technique. For these proceedings we will briefly recapitulate that summary in the course of an evaluation of the role that ARPEFS analysis can play in surface structure determination.

## Small Atom Approximation Formula

The simplest theoretical treatment for ARPEFS predicts intensity oscillations according to

$$I(E) \doteq I_0(E) + X(E)I_0(E) \tag{1}$$

where $I(E)$ is the measured photocurrent, $I_0(E)$ is the atomic cross section and

$$X(k) = 2 \sum_j \frac{\cos \beta_j}{\cos \gamma} \frac{|f(\alpha_j)|}{r_j} \cos(k(r_j - r_j \cos \alpha_j) + \phi_j) \; . \tag{2}$$

where the photoelectron wave encounters an ion core at a distance $r_j$ from the source atom, scatters through an angle $\alpha_j$ with amplitude $|f(\alpha_j)|$, and, after a phase shift $\phi_j$, propagates towards the detector. The angle between the polarization direction and the direct emission path is $\gamma$; the angle between the polarization direction and the

DISTRIBUTION OF THIS DOCUMENT IS UNLIMITED

initial path of an electron scattered from site j is $\alpha_j$. Figure 1 shows the scattering geometry and Figure 2 illustrates typical scattering angular distributions. The wavenumber, k, and the kinetic energy E are connected by the de Broglie relation

$$k^2 = \frac{2m}{\hbar^2}(E-E_0). \quad (3)$$

This formula contains the essential aspects of photoelectron diffraction for kinetic energy above 50 eV, but it makes assumptions which may not always be valid. The most important approximations are:

i) small atom approximation. The scattering potential has been concentrated at a point and the variation of the wave amplitude across the potential has been ignored.
ii) muffin tin potential. The potentials are central and do not overlap.
iii) elastic, potential scattering. Inelastic scattering, charge state of the scattering atom, exchange, and randomized atomic positions have been ignored.
iv) fully screened sudden approximation final state. The interaction of the hole with the photoelectron has been ignored, and
v) single scattering.

These approximations[14] are substantiated experimentally in the highly successful extended x-ray absorption fine structure (EXAFS) technique. However, EXAFS relies on empirical phase shift transferability, and it is not physically identical to ARPEFS: we take the EXAFS evidence for the form of equation 2 but the scattering amplitude and phase may not be that predicted by the small atom theory.

This ARPEFS formula suggests that the proportional change in photoemission intensity is as large as the elastic scattering power $|f(\alpha_j,k)|$ times the number of scatterers and that the oscillations are cosinusoidal when expressed as a function of wavenumber k. Figures 3 and 4 substantiate these predictions: the oscillations are > 50 percent and appear to be dominated by a few constant frequencies.

More quantitative analysis of the oscillations as a function of energy is difficult. Each region of the ARPEFS curve contains signal contributions from all scattering atoms. We therefore turn to the Fourier representation.

## Fourier Analysis of ARPEFS

The cosinusoidal form of the ARPEFS suggests that a Fourier transform of these oscillations will be peaked near $r_j - r_j \cos \alpha_j$, provided that i) the scattering power, $f(\alpha_j k)$ , is structureless in energy, ii) the scattering phase, $\phi_j$, is nearly linear, and iii) the measured energy range is long enough to give sharp Fourier features. Again EXAFS experience encourages our work, but ARPEFS path-length differences can vary continuously from 0 to $2r_j$: depending on the scattering angle $\alpha_j$ many Fourier peaks can result. Fortunately, the scattering power is strongly peaked[11] and the final state dependence (in cos $\beta_j$) contains sharp nodes: some path lengths will have too little amplitude to give a Fourier peak.

Nevertheless, traditional Fourier transformation methods will not provide sufficient resolution with the typical ARPEFS energy range of ~ 500 eV. Thus, we have adapted the auto-regressive or maximum entropy spectral analysis technology[10] to extract the maximum reliable resolution from our data. The $X(k)$ curve is fit to an auto-regressive function and this function is extrapolated. The resulting longer "data" train is then processed in the traditional fashion. The procedure can be viewed as an improved method for minimizing edge or truncation effects in the Fourier transform.[15]

Auto-regressive Fourier transforms of S(1s) ARPEFS from p(2x2)S/Cu(100) measured along [110] and c(2x2)S/Ni(100) measured along [110] and along [100] are shown in Figure 5. These spectra illustrate three types of structural information which can be derived from ARPEFS. We will discuss these spectra in the next section.

## Interpretation of the Fourier Spectra

Equation 2 predicts that ARPEFS Fourier transforms will be peaked near $r_j - r_j \cos \alpha_j$ with an amplitude which depends on the scattering angle $\alpha_j$ and on $\beta_j$, the angle between the polarization vector and the scattering atom position.

The Fourier <u>peak position</u> corresponds to a path-length difference, $r_j - r_j \cos \alpha_j$. This difference contains information about the scattering atoms' distance from the emitter and orientation with respect to the detector. As comparison of figure 5b and

5c shows, different emission angles will give different Fourier spectra. We first discuss the [110] emission direction ARPEFS Fourier transform given in Fig 5b.

There are five peaks below 10 Å path-length difference in Fig. 5b. We assign the first three peaks to nearest neighbors: i) the peak at 1.9 Å corresponds to the atom closest to the detector along [$\bar{1}$10] ($\alpha_j = 83^\circ$), ii) the peak at 3.2 Å corresponds to two atoms above and below the plane of figure 1 ($\alpha_j = 116^\circ$) and, iii) the peak at 4.5 Å corresponds to the atom behind the sulfur from the detector ($\alpha_j = 173^\circ$). We have isolated the third peak, backtransformed it and removed the Ni backscattering phase to obtain a bond length of 2.23 Å, in agreement with literature values[16].

The two remaining peaks in the Fourier spectrum belong to backscattering atoms further along [110] from the detector, but several atoms contribute to each peak.

Figure 5(a) displays the same type of spectrum but measured for p(2x2)S/Cu(100). It is immediately evident that S sits in a four-fold hollow site at a distance not too different from sulfur on Ni. Further the great similarity of these spectra suggests limited scattering occurs from other sulfur adsorbate atoms: The p(2x2) overlayer contains half as many sulfur atoms.

*In* addition to structure information in the path length differencs, we can examine the Fourier peak area. The area is proportional to both the scattering power, $|f(\alpha_j)|$, and the amplitude of the final state wavefunction in the region of the scattering atom, $\cos\beta_j/\cos\gamma$. We can rationalize the first three peak heights observed for S/Ni-[$\bar{1}$10] in the following manner:

i) the first peak is very small because $\cos 83^\circ = .12$,
ii) the third peak is large because $f(\alpha_j)$ peaks at $180^\circ$ and $\cos 173^\circ/\cos\gamma = -1$, and
iii) the second peak has two atoms at $\cos 116^\circ = -.4$; it is smaller than the third peak by roughly the ratio of the scattering power at $116^\circ$ to the power at $180^\circ$.

Comparison of the *S/Ni curve (fig 5b) and S/Cu curve (fig 5a) further supports* the peak assignments. For the S/Cu measurements the polarization vector was tipped $15^\circ$ closer to the surface. While this change had little effect on the amplitude at $116^\circ$ and $173^\circ$, the first peak amplitude rose from $\cos 83^\circ/\cos 0^\circ$ to $\cos 68^\circ/\cos 15^\circ$; the increase is a factor of 3. The increase is evident as the major difference (aside from slightly better resolution for S/Cu) between the two curves.

The third panel of Fig. 5 illustrates the one exception to the simple picture of Fourier peak position and amplitude. This curve is a normal emission [100] ARPEFS Fourier transform. We can assign the major peak at 6.2 Å as scattering from five atoms in the second Ni layer, but the four nearest-neighbor path lengths should be 3.6 Å: no peak appears here while two unassigned peaks surround 3.6 Å.

Both unassigned peaks are due to nearest-neighbor scattering, but the scattering angle of $128^\circ$ leads to a scattering amplitude with a generalized Ramsauer-Townsend "anti-resonance"[13]. The scattering power goes to zero near the center of the ARPEFS spectrum, and the scattering phase sweeps rapidly through $\pi$. This structure in the scattering amplitude splits the Fourier peak.

The generalized Ramsauer-Townsend effect is very sensitive to the scattering angle as indicated in Fig. 6. This Fourier peak splitting may be an avenue to a method for measuring bond angles. We are currently investigating this effect and we have already discovered that the small atom theory is not adequate for quantitative calculation near resonance.

## Current Status and Role of ARPEFS

The results presented in the previous section bring photoelectron diffraction out of an era of trial-and-error comparison of data to theory. The direct analysis provided by the Fourier transform and single scattering formula puts the experimentalist in control of the structural determination. To conclude this paper, we briefly describe the properties of angle-resolved photoemission extended fine structure and discuss the class of structural problems for which ARPEFS would be particularly suited.

Photoemission is essentially non-destructive; photon beam exposure has little effect *on even reactive molecular adsorbates.* For the kinetic energies 50-500 eV used in ARPEFS, the surface sensitivity is high, although it falls at the upper extreme. Core level lines are sharp features easily followed when the photon energy is scanned.

Photoemission intensity is proportional to the concentration of adsorbed species and hence ARPEFS reports on the majority surface species. The ARPEFS interference requires each adsorbate site to be oriented the same with respect to the detector.

Primary among the advantages of photoemission is the high chemical selectivity. Each element of an adsorbate molecule can be individually probed. Chemically shifted core levels and surface core level shifts provide opportunities for further selectivity.

The angle-resolved nature of ARPEFS provides further criteria for applications. Independent control of the polarization and emission direction allows many different views of an adsorbate system; each view can provide more clues to a surface structure. Since only intensities are affected by moving the polarization vector and by using a different adsorbate core level, Fourier peaks can be emphasized or eliminated easily.

The direct wave-scattered wave interference basis of ARPEFS guarantees that the oscillations will be large, and that the physical nature of the scattering can be studied in a straightforward manner. Indeed one of the interesting scattering effects--the generalized Ramsauer-Townsend effect--may lead to an accurate method for bond angle determination.

With these considerations, we briefly recall the advantages of the other two most used structure methods: Low Energy Electron Diffraction (LEED) and Surface Extended X-Ray Absorption Fine Structure (SEXAFS).

LEED continues to make steady progress. The advent of high gain detectors reduces the electron beam damage effects that previously limited this technique. Theoretical refinements[17,18] have improved the prospects for solving more complicated structures. The major strength of LEED--experimental simplicity--must be balanced against the complexity of its analysis. Clearly the large number of simple structures solved by LEED suggests that for these systems the complexity is tractable.

Surface EXAFS[16] has made giant strides since its introduction. In return for venturing to a synchrotron storage ring, SEXAFS provides direct structure analysis including highly accurate bond lengths without requiring an ordered overlayer structure. The key advantage of SEXAFS--direct measurement of an average bond length to nearest neighbors--is also its key weakness for complicated structures. A well characterized but complex adsorbate could have many similar bond lengths which SEXAFS cannot resolve. For disordered systems, however, the average bond length may be the only useful parameter to describe the structure, and SEXAFS would be uniquely suitable.

We have demonstrated that ARPEFS can elegantly solve simple surface structures such as the p(2x2)S/Cu(100) structure in Figure 5a. However, the surface EXAFS measurement would have been much easier to analyze and LEED could have been used to solve the structure with commercially available instruments. ARPEFS measurements for this class of surface structure seem unduly complicated.

Atomic systems which will benefit from the advantages of ARPEFS include:

i) (111) surfaces where two different three-fold hollow sites have similar nearest neighbor distances but are distinguished by second layer substrate atoms. Normal emission ARPEFS would be ideal for scattering from the second layer atom.

ii) Multiple site adsorption. More than one occupied site will likely have similar bond lengths but very different path-length differences in some directions.

iii) Atoms on stepped surfaces. Here the high angle selectivity would be valuable to concentrate on only the atoms on the edges.

Beyond atomic systems, the more complicated the adsorbate molecule, the more advantages of ARPEFS will be evident. ARPEFS can dissect a molecular adsorbate structure problem by examining each element from each of several different view points. Surface structures of molecules larger than diatomics are essential to chemical studies of surfaces. With direct analysis, ARPEFS is capable of determining these structures with only synchrotron radiation beam time limiting the applications. With the imminent availability of soft x-rays at Brookhaven and the advent of ultra bright light sources, such as Lawrence Berkeley Laboratory's Advanced Light Source, this limitation should be removed.

## Acknowledgements

This work was supported by the Director, Office of Energy Research, Office of Basic Energy Sciences, Chemical Sciences Division of the U.S. Department of Energy under *Contract No. DE-AC03-76SF00098. It was performed at the Stanford Synchrotron Radiation* Laboratory, which is supported by the NSF through the Division of Materials Research.

## References

*Department of Physics, University of Petroleum and Minerals, Dhahran, Saudi Arabia.

1. S.D. Kevan, D.H. Rosenblatt, D. Denley, B.-C. Lu, and D.A. Shirley, Phys. Rev. Lett. 41, 1565 (1978).
2. a) S. Kono, C.S. Fadley, N.F.T. Hall, and Z. Hussain, Phys. Rev. Lett. 41, 117 (1978); b) S. Kono, S.M. Goldberg, N.F.T. Hall, and C.S. Fadley, Phys. Rev. Lett. 41, 1831 (1978).
3. D.P. Woodruff, D. Norman, B.W. Holland, N.V. Smith, H.H. Farrell, M.M. Traum, Phys. Rev. Lett. 41, 1130 (1978).
4. A. Liebsch, Phys. Rev. Lett. 32, 1203 (1974).
5. P.A. Lee, Phys. Rev. B 13, 5261 (1976).
6. a) S.Y. Tong, C.H. Li, and A.R. Lubinsky, Phys. Rev. Lett. 39, 498 (1977); b) C.H. Li, A.R. Lubinsky, and S.Y. Tong, Phys. Rev. B 17, 3128 (1978).
7. a) S.D. Kevan, D.H. Rosenblatt, D.R. Denley, B.-C. Lu, Phys. Rev. B 20, 4133 (1979); b) S.D. Kevan, J.G. Tobin, D.H. Rosenblatt, R.F. Davis, and D.A. Shirley, Phys. Rev. B 23, 493 (1981); c) S.D. Kevan, R.F. Davis, D.H. Rosenblatt, J.G. Tobin, M.G. Mason, D.A. Shirley, C.H. Li, and S.Y. Tong, Phys. Rev. Lett. 46, 1629 (1981); d) D.H. Rosenblatt, S.D. Kevan, J.G. Tobin, R.F. Davis, M.G. Mason, D.R. Denley, D.A. Shirley, Y. Huang, and S.Y. Tong, Phys. Rev. B 26, 1812 (1982); D.H. Rosenblatt, J.G. Tobin, M.G. Mason, R.F. Davis, S.D. Kevan, D.A. Shirley, C.H. Li, and S.Y. Tong, Phys. Rev. B 23, 3828 (1981).
8. J.J. Barton, C.C. Bahr, Z. Hussain, S.W. Robey, J.G. Tobin, L.E. Klebanoff, and D.A. Shirley, Phys. Rev. Lett. 51, 272 (1983).
9. Z. Hussain, E. Umbach, D.A. Shirley, J. Stohr, and J. Feldhaus, Nucl. Instrum. Methods 195, 115 (1982).
10. J.J. Barton and D.A. Shirley, to be published.
11. P.J. Orders and C.S. Fadley, Phys. Rev. B 27, 781 (1983).
12. J.J. Barton and D.A. Shirley, in preparation.
13. J.J.Barton, C.C. Bahr, Z. Hussain, S.W. Robey, L.E. Klebanoff, and D.A. Shirley, J. Vac. Sci. Technol., to be published.
14. B.A. Bunker and E.A. Stern, Phys. Rev. B 27, 1017 (1983).
15. S.M. Kay and S.L. Marple, Proc. IEEE 69, 1380 (1981).
16. S. Brennan, J. Stöhr, and R. Jaeger, Phys. Rev. B 24, 4871(1981), and references therein.
17. W.S. Yang, F. Jona, and P.M. Marcus, Phys. Rev. B 28, 2049 (1983).
18. M.A. Van Hove, R. Lin, and G.A. Somorjai, Phys. Rev. Lett. 51, 778 (1983).

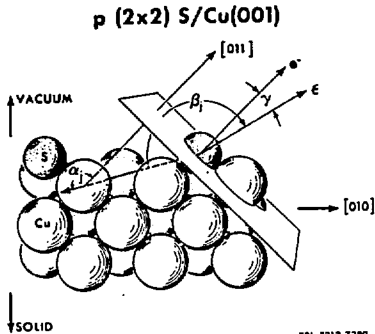


Figure 1. Cross-sectional view of a fcc crystal (001) surface showing the experimental geometry and illustrating the parameters of the analytic single-scattering formula. The angle-resolved detector is along the vector labeled $e^-$ ([011] direction); the polarization vector is $\vec{\varepsilon}$. The angle between these two vectors is $\gamma$. The vector from the emitter to the scattering atom j makes an angle $\beta_j$ with the polarization vector and an angle $\alpha_j$ with the emission direction.

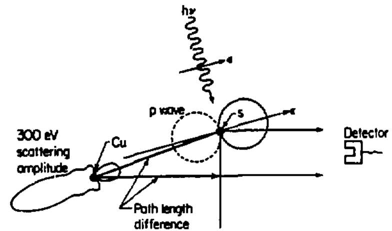


Figure 2. Illustration of the scattering process. The direct wave has an angular distribution dependent upon the initial state (1s) and the photon polarization direction, $\vec{\varepsilon}$. The scattering from each atomic center depends upon its scattering angle $\alpha_j$. The scattering amplitude calculated for 300 eV is shown superimposed on the scattering atom. This amplitude is strongly peaked in the forward and backward directions. The geometric path-length difference is also illustrated.

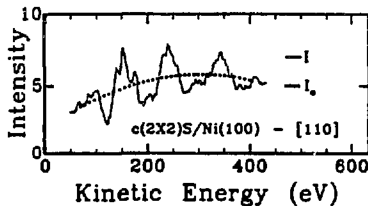


Figure 3. Photoemission partial-cross-section measurements for c(2x2)S/Ni(100). The curve I represents the area of the elastic photopeak, divided by the background emission to correct for photon flux, multiplied by kinetic energy to correct for electron-analyzer transmission, and divided by 100,000.

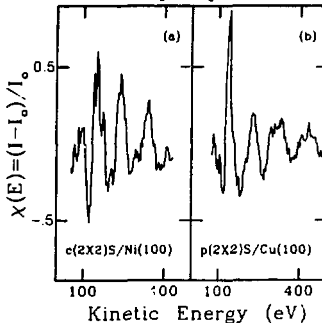


Figure 4. ARPEFS modulations derived from S(1s) photoemission partial cross-sections. Both curves were measured with the detector along a [110] direction from a (100) surface; a) c(2x2)S/Ni(100); b) p(2x2)S/Cu(100).

Figure 5. Auto-regressive Fourier transforms of the three ARPEFS curves discussed in the text. Note that a path-length difference of 4.4 Å corresponds to a bond length of 2.2 Å when $\alpha_j$ = 173°. (a) S(1s) ARPEFS from p(2x2)S/Cu(100); detector along [110], γ = 15°, (b) S(1s) ARPEFS from c(2x2)S/Ni(100); detector along [110], γ = 0°, (c) S(1s) ARPEFS from c(2x2)S/Ni(100); detector along [100] (normal emission), γ = 20°. In all curves the intensity below 1.5 Å varies with the background function choice and has been disregarded.

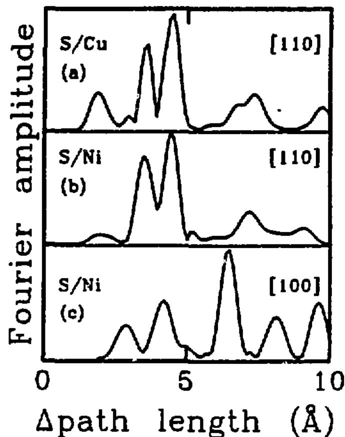


Figure 6. Ni scattering amplitude phase shifts using the small atom (plane wave) approximation. Four angles near the generalized Ramsauer-Townsend zero crossing are plotted. *All four begin with a phase* shift near .5 radians at 4 $Å^{-1}$ and end near ± 3.1 rad., but in the region of the resonance the behavior depends strongly on scattering angle.

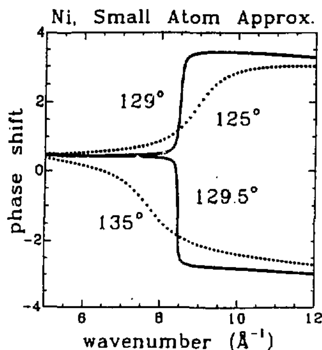

This report was done with support from the Department of Energy. Any conclusions or opinions expressed in this report represent solely those of the author(s) and not necessarily those of The Regents of the University of California, the Lawrence Berkeley Laboratory or the Department of Energy.

Reference to a company or product name does not imply approval or recommendation of the product by the University of California or the U.S. Department of Energy to the exclusion of others that may be suitable.